ResearchGate

See discussions, stats, and author profiles for this publication at: https://www.researchgate.net/publication/374049655

Liquid crystal-enabled tunability of Yagi-Uda antenna resonant properties

Article *in* Journal of Optical Microsystems · September 2023

DOI: 10.1117/1.JOM.3.4.041203

CITATION
1

READS
133

2 authors:

Ivan I Yakovkin
Taras Shevchenko National University of Kyiv
41 PUBLICATIONS **69** CITATIONS
SEE PROFILE

Victor Yu. Reshetnyak
369 PUBLICATIONS **4,396** CITATIONS
SEE PROFILE

All content following this page was uploaded by Ivan I Yakovkin on 21 September 2023.

The user has requested enhancement of the downloaded file.

JOM Journal of Optical Microsystems

RESEARCH PAPER

Liquid crystal-enabled tunability of Yagi-Uda antenna resonant properties

Ivan Yakovkin[a,*] **and Victor Reshetnyak**[a,b]

[a]Taras Shevchenko National University of Kyiv, Physics Faculty, Kyiv, Ukraine
[b]University of Leeds, School of Physics and Astronomy, Leeds, United Kingdom

ABSTRACT. We demonstrate the application of liquid crystals to modulate the resonance properties of Yagi-Uda metamaterial absorbers. The absorbance and reflectance peak frequencies and amplitudes were found to be adjustable by reorienting the liquid crystal, irrespective of the polarization of the incident light. Notably, the lowest resonant frequencies were observed when the liquid crystal was in the homeotropic orientation, whereas a reorientation toward the *y*-axis showed a significant frequency increase, up to 1 GHz. Incorporating liquid crystals to the Yagi-Uda antenna arrays can also serve as a method for eliminating undesired modes, not associated with the antenna resonance. This can be achieved by taking advantage of the sensitivity differences of these modes to refractive index components. The results presented in this study highlight the potential of liquid crystals to deliver dynamic manipulation and real-time adaptability of Yagi-Uda antennas.

© The Authors. Published by SPIE under a Creative Commons Attribution 4.0 International License. Distribution or reproduction of this work in whole or in part requires full attribution of the original publication, including its DOI. [DOI: 10.1117/1.JOM.3.4.041203]

Keywords: Yagi-Uda antenna arrays; metamaterials; liquid crystals; controllable reflectance

Paper 23010SS received Jun. 2, 2023; revised Aug. 21, 2023; accepted Sep. 6, 2023; published Sep. 19, 2023.

1 Introduction

Metamaterials have been at the forefront of recent scientific exploration. These materials have demonstrated capabilities, such as negative refraction, cloaking, advanced lensing, dynamically tunable plasmon-induced transparency, and perfect absorption.[1–7] Unlike traditional materials, the distinguishing attributes of metamaterials stem not from their elemental composition, but rather from their meticulously designed structure.[8–14] This structural dependency of their properties offers potential for designing groundbreaking devices catering to various microwave and optical applications.[15–25]

Among the various types of metamaterials, perfect metamaterial absorbers (PMAs) have attracted significant attention.[26–28] Recent research has broadened the scope of PMAs, culminating in the design of absorbers capable of functioning across diverse regions of the electromagnetic spectrum, including microwave, millimeter-waves, terahertz, and visible regimes.[29–33]

In the realm of microwave absorbers, structures based on meander wire and high length-diameter ratio iron nanowires have showcased exemplary absorption performances.[34,35] In the terahertz regime, researchers have made significant strides in designing absorbers using materials such as graphene.[30] In addition, within the visible spectrum, nanostructured elements have been leveraged to create efficient absorbers, further demonstrating the versatility of these structures.[31,33]

*Address all correspondence to Ivan Yakovkin, yakovkinii@gmail.com

Downloaded From: https://www.spiedigitallibrary.org/journals/Journal-of-Optical-Microsystems on 19 Sep 2023
Terms of Use: https://www.spiedigitallibrary.org/terms-of-use

In particular, Yagi-Uda structures have drawn attention due to their inherent resonance capabilities and directionality, properties that make them effective absorbers for selected wavelengths.[36,37] This has allowed for the extension of their application beyond traditional communication systems to fields, such as electromagnetic interference reduction and stealth technology.

In the study by Bilal et al.,[38] a multiband Yagi-Uda shaped metamaterial absorber (YUMA) operating in X- and Ku-bands of the microwave spectrum was introduced. Exhibiting three distinct absorption peaks at 10.64, 12.08, and 14.09 GHz, the YUMA has shown polarization controllability and wide incidence angle stability. Mutual coupling between the arms of the Yagi-Uda structure was found to contribute significantly to the multiband absorption mechanism, suggesting potential applications for the YUMA in X- and Ku-band operations.

In this paper, the capabilities of Yagi-Uda metamaterial absorber are augmented by integrating liquid crystals (LCs) into their design. This approach provides the potential for dynamic manipulation of antenna properties, thereby enabling real-time adaptability based on the operational needs.

2 Configuration of Yagi-Uda Antenna Metamaterial Absorber

We introduce dynamic control and tunability to the Yagi-Uda antenna array by incorporating LCs, extending the design discussed in Ref. 38 The Yagi-Uda antenna array exhibits the following properties as shown in Fig. 1.

The Yagi-Uda antenna array, constructed of pure metallic copper with an electric conductivity (σ) of 5.8×10^7 S/m, is located atop a dielectric slab substrate. The substrate, which also employs a thin 0.035 mm copper film as a ground plane, has a thickness h_s of 1.6 mm. The antenna array itself is made up of multiple elements, each with specific dimensions. The length of the antenna L is set at 9 mm, while the five perpendicular conducting arms have lengths of 4 mm (L_1), 3.5 mm (L_2), 3 mm (L_3), 2.5 mm (L_4), and 2 mm (L_5), respectively. All elements of the antenna array, including the antenna and its arms, have a width W of 0.5 mm. The thickness of the antenna is 0.035 mm.

Above the Yagi-Uda antenna, the space is filled with a semi-infinite high-birefringence LC. The birefringence of LCs can be as high as $\Delta n \approx 0.8$[39,40] and is likely to reach an even higher value of 0.9.[41] In order to highlight the potential impact of the LC orientation on the properties of the Yagi-Uda antenna arrays, a LC with an ordinary refractive index n_o of 1.7 and an extraordinary index n_e of 2.7 was considered. The dielectric material used to separate the copper structures is FR-4. This substrate material has a relative permittivity ε_r of 4.3 and a loss tangent tan δ of 0.025. The dimensions of the unit cell span a size P of 12 mm in both the x and y directions. The Floquet periodic boundary conditions for the unit cell are applied in the x and y directions, while an open add space boundary condition is simulated along the z direction using perfectly

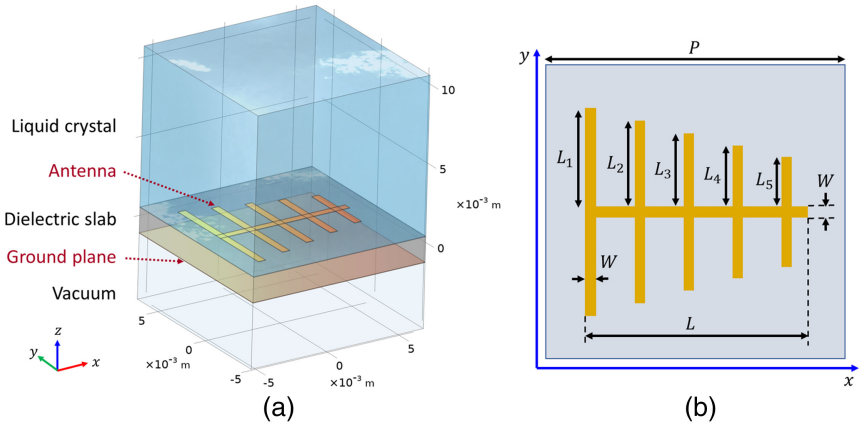

Fig. 1 (a) Unit cell with a Yagi-Uda antenna in contact with LC and (b) detailed dimensions of the antenna used in calculations.

Downloaded From: https://www.spiedigitallibrary.org/journals/Journal-of-Optical-Microsystems on 19 Sep 2023
Terms of Use: https://www.spiedigitallibrary.org/terms-of-use

matched layers. The calculations were performed using the finite element method in COMSOL Multiphysics.

To demonstrate the capability of using LCs to adjust the resonance properties of Yagi-Uda antennas, we conducted a comparison of the absorbance and reflectance spectra of Yagi-Uda antenna arrays under of the x- and y-polarized plane waves propagating in the $-z$ direction. We examined three distinct orientations of the LCs: homeotropic ($\vec{n}||z$) and two planar orientations ($\vec{n}||x$ and $\vec{n}||y$) where $\vec{n}$ represents the LC director.

The reorientation can be set up using in-plane electrodes or through photo-orientation methods.[42,43] Reorientation can also be achieved by employing a magnetic field. It should be noted that boundary conditions can prevent the LC from reorienting at the substrate. However, using a photoalignment layer over the electrodes can allow for complete reorientation.[44] Overall, this approach serves as a proof of concept, confirming the feasibility of utilizing LCs for tuning Yagi-Uda antennas.

3 Absorption and Reflectance for x-Polarized Incident Light

Figure 2 shows the reflectance and absorbance spectra for an x-polarized plane wave of normal incidence. As expected from such antennas, the spectra consist of multiple discrete absorption peaks that correspond to the resonant frequencies of different antenna elements. The effect of reorienting the LC from a homeotropic to a planar state in the $x-z$ plane is manifested as a gradual increase of the width of the absorption peaks, accompanied by a minor increase in the resonant frequency by $\sim$0.1 GHz.

On the other hand, the reorientation from the homeotropic to the planar state in the $y-z$ plane has a significant impact on the resonance frequencies by shifting them by approx. 1 GHz to the larger frequencies, accompanied by a slight increase in peak widths. As such, altering the y-component of the LC director significantly changes the resonant frequency, while balancing x and z components can be utilized for fine-tuning the absorption profiles.

To comprehend the response of the YUMA to the LC reorientation, it is crucial to examine the polarization and spatial distribution of the electric field in the Yagi-Uda structures (Fig. 3). One of the critical features of the YUMA is its ability to convert the polarization of incident light. Although the incident light only exhibits the x-component of the electric field vector, all three components are present near the antenna, with x and y being dominant. This allows the absorbance and reflectance to be dependent on the y and z components of the refractive index, i.e., on the reorientation of the director in the $y-z$ plane.

The analysis of the modes shows that x- and y-polarized modes behave quite differently. The x-polarized modes are found along the antenna arms, while the y-polarized modes localize near the tips of the arms. These y-polarized modes define the resonant frequency as they are sensitive to the length of the antenna arms and their polarization makes them responsive to the y-component of the refractive index of the surrounding media, including the LC. The YUMA sensitivity to the y-component of the director, and much less sensitivity to the x and z components, results in a significant shift of the absorbance peaks' frequency for the y-planar orientation.

A separate analysis should be made for the mode around 14 GHz (Fig. 2). The distribution of components of the electric field (Fig. 3, bottom row) reveals that this mode is z-polarized and does not correspond to the antenna-arm-length-related resonance. This mode is associated with the periodicity of the entire structure. The resonance frequency can be roughly estimated by matching the wavelength of a z-polarized plane wave with the width of the cell:

$$f = \frac{c}{n_o P} \approx 14.7 \text{ GHz}.$$

Since the 14 GHz mode is z-polarized, it is highly sensitive to the reorientation of the LC between planar and homeotropic states. Transitioning between the two planar states has a slight impact on the mode's frequency, while switching to the homeotropic orientation drastically changes the resonant frequency, effectively disabling this resonance peak. Given the significant influence of LC orientation in both the $x-z$ and $y-z$ planes on this mode, and the more gradual

Downloaded From: https://www.spiedigitallibrary.org/journals/Journal-of-Optical-Microsystems on 19 Sep 2023
Terms of Use: https://www.spiedigitallibrary.org/terms-of-use

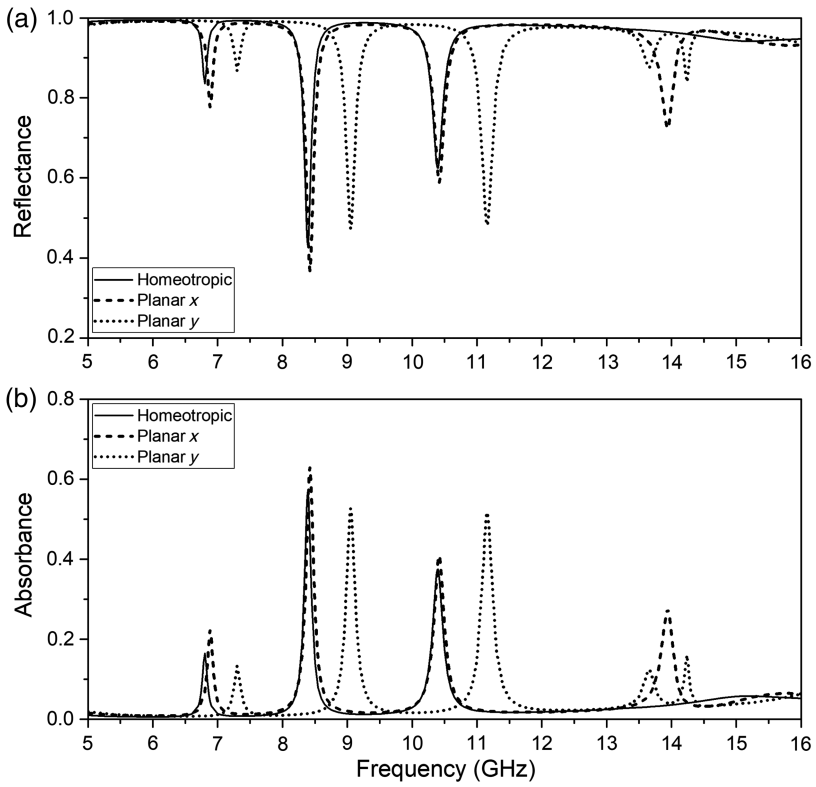

Fig. 2 (a) Reflectance and (b) absorbance spectra for the case of *x*-polarized incident plane wave.

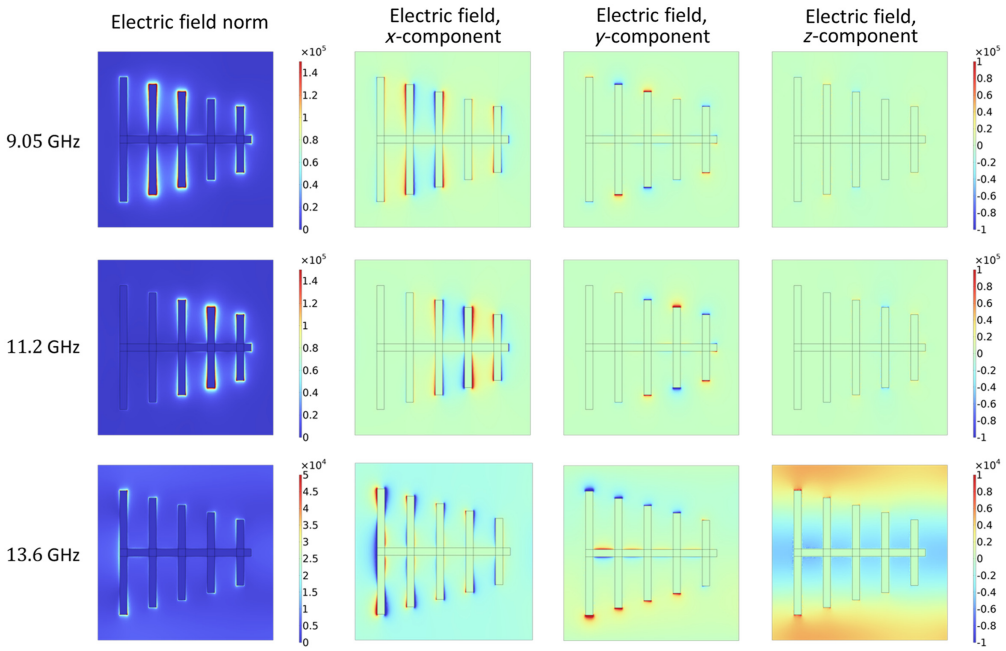

Fig. 3 Electric field distributions at frequencies corresponding to absorption peaks for the case of *x*-polarized incident light with the planar LC orientation along the *y* axis.

response of the Yagi-Uda antenna resonances to $x - z$ reorientation, adjusting the LC orientation in the $x - z$ plane can be utilized to manipulate the relative position of these modes. This can be employed to either distance of the antenna from undesired modes or, conversely, to enable a controlled overlap of such modes.

Downloaded From: https://www.spiedigitallibrary.org/journals/Journal-of-Optical-Microsystems on 19 Sep 2023
Terms of Use: https://www.spiedigitallibrary.org/terms-of-use

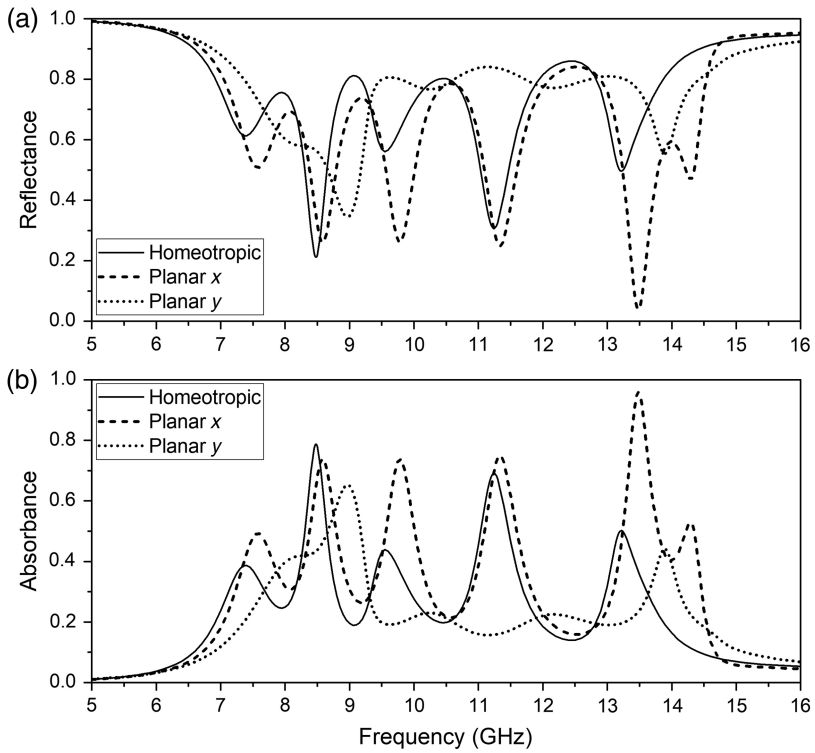

Fig. 4 (a) Reflectance and (b) absorbance spectra for the case of *y*-polarized incident plane wave.

4 Absorbance and Reflectance for *y*-Polarized Incident Light

Figure 4 shows the reflectance and absorbance spectra in the context of *y*-polarized plane wave. The YUMA shows five absorption peaks corresponding to the five arms of the Yagi-Uda structure. In a manner akin to the *x*-polarization scenario, the transition of the LC from the homeotropic to the planar state in the $x - z$ plane results in a slight escalation in the resonant frequency, accompanied by a redistribution of peak heights.

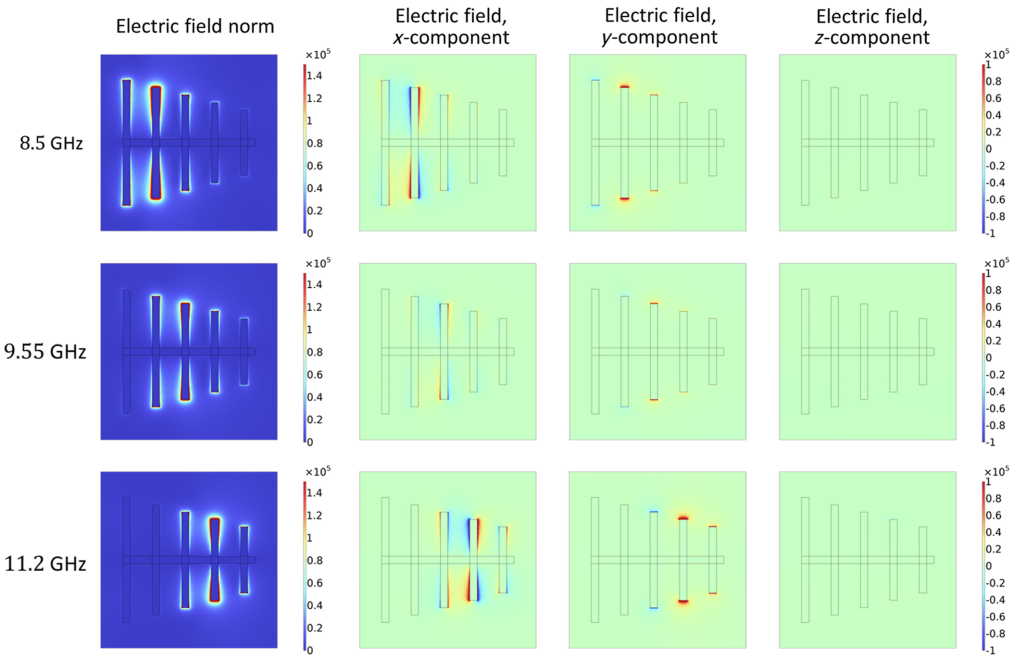

Fig. 5 Electric field distributions at frequencies corresponding to absorption peaks for the case of *y*-polarized incident light and homeotropically aligned LC.

Downloaded From: https://www.spiedigitallibrary.org/journals/Journal-of-Optical-Microsystems on 19 Sep 2023
Terms of Use: https://www.spiedigitallibrary.org/terms-of-use

When the director orientation transitions toward the y-direction, a significant increase in resonant frequencies – up to 1 GHz – is noted. This shift is accompanied by a drastic reduction in the amplitudes of the higher frequency peaks. The 14.3 GHz peak, similar to the x-polarization case, is associated with the width of the unit cell. The behavior of this mode aligns qualitatively with its counterpart in the x-polarization scenario.

Electric field distributions for the three central absorption peaks are presented in Fig. 5. By comparing Figs. 3 and 5, it becomes clear that the change in polarization of the incident wave introduces a different parity to the electric field distribution. For the incident x-polarization (Fig. 3), the x-component of the electric field distribution is symmetric, and the y-component is antisymmetric, relative to the primary antenna axis. Conversely, in the case of y-polarized incident wave (Fig. 5), the x-component of the excited mode is antisymmetric, and the y-component is symmetric relative to the antenna axis.

Furthermore, it is evident that the resonances in the case of x-polarized incident light involve multiple antenna arms simultaneously, while in the case of y-polarized incident wave the modes have a clear one-to-one correspondence between an antenna arm and the peak of the mode field distribution.

5 Conclusions

We have demonstrated the potential of LC in fine-tuning the resonance properties of Yagi-Uda antenna arrays. In both scenarios of incident light, x- and y-polarization (parallel and perpendicular to the antenna symmetry axis), the reorientation of the LC allows for control over the frequency of absorbance and reflectance peaks. The homeotropic orientation of the LC resulted in the lowest resonant frequencies, while the reorientation of the LC director toward the y-direction leads to a substantial increase in the resonant frequencies, by up to 1 GHz.

In addition, it was found that different types of modes had different levels of sensitivity to different refractive index components, allowing for unwanted modes to be shifted away from specific frequency ranges of interest. This study serves as a proof of concept for using LCs to augment and manipulate Yagi-Uda metamaterial absorbers in real-time, granting more control over their resonance properties.

Code, Data, and Materials Availability

Data underlying the results presented in this paper are not publicly available at this time but may be obtained from the authors upon reasonable request.

Acknowledgments

The authors declare no conflicts of interest.

References

1. D. R. Smith et al., "Composite medium with simultaneously negative permeability and permittivity," *Phys. Rev. Lett.* **84**(18), 4184–4187 (2000).
2. Y. Ra'di, C. R. Simovski, and S. A. Tretyakov, "Thin perfect absorbers for electromagnetic waves: theory, design, and realizations," *Phys. Rev. Appl.* **3**(3), 037001 (2015).
3. J. B. Pendry, "Negative refraction makes a perfect lens," *Phys. Rev. Lett.* **85**(18), 3966–3969 (2000).
4. D. Schurig et al., "Metamaterial electromagnetic cloak at microwave frequencies," *Science* **314**(5801), 977–980 (2006).
5. R. M. H. Bilal et al., "Tunable and switchable bifunctional meta-surface for plasmon-induced transparency and perfect absorption," *Opt. Mater. Express* **12**(2) 798–810 (2022).
6. B. A. Munk, *Metamaterials: Critique and Alternatives*, p. 189, John Wiley & Sons (2009).
7. F. Capolino, *Theory and Phenomena of Metamaterials*, 1st ed., CRC Press (2009).
8. S. Burgos et al., "A single-layer wide-angle negative-index metamaterial at visible frequencies," *Nat. Mater.* **9**, 407–412 (2010).
9. Q.-Y. Wen et al., "A tunable hybrid metamaterial absorber based on vanadium oxide films," *J. Phys. D: Appl. Phys.* **45**, 235106 (2012).
10. S. Yang et al., "From flexible and stretchable meta-atom to metamaterial: a wearable microwave meta-skin with tunable frequency selective and cloaking effects," *Sci. Rep.* **6**, 21921 (2016).

Downloaded From: https://www.spiedigitallibrary.org/journals/Journal-of-Optical-Microsystems on 19 Sep 2023
Terms of Use: https://www.spiedigitallibrary.org/terms-of-use

11. T. Matsui et al., "Reflection-less frequency-selective microwave metamaterial absorber," *OSA Contin.* **4**, 2351–2363 (2021)
12. W. Chen et al., "Controlling gigahertz and terahertz surface electromagnetic waves with metamaterial resonators," *Phys. Rev. X* **1**, 0210162 (2011).
13. C. Soukoulis and M. Wegener, "Past achievements and future challenges in the development of three-dimensional photonic metamaterials," *Nat. Photonics* **5**, 523–530 (2011).
14. R. McPhedran et al., "Metamaterials and metaoptics," *NPG Asia Mater.* **3**, 100–108 (2011).
15. P.-A. Yang et al., "Optimization of Fe@Ag core–shell nanowires with improved impedance matching and microwave absorption properties," *Chem. Eng. J.* **430**, 132878 (2022).
16. A. Krasnok et al., "Anomalies in light scattering," *Adv. Opt. Photonics* **11**(4), 892–951 (2019).
17. M. A. Naveed et al., "Optical spin-symmetry breaking for high-efficiency directional helicity-multiplexed metaholograms," *Microsyst. Nanoeng.* **7**(1), 5–9 (2021).
18. I. S. Maksymov et al., "Optical Yagi-Uda nanoantennas," *Nanophotonics* **1**(1), 65–68 (2012).
19. J. Sol, D. R. Smith, and P. del Hougne, "Meta-programmable analog differentiator," *Nat. Commun.* **13**, 1713 (2022).
20. A. Valipour et al., "Metamaterials and their applications: an overview," *Proc. Inst. Mech. Eng., Part L: J. Mater.: Des. Appl.* **236**(11), 2171–2210 (2022).
21. M. Hussain et al., "Metamaterials and their application in the performance enhancement of reconfigurable antennas: a review," *Micromachines* **14**(2), 349 (2023).
22. P. W. Kolb et al., "Extreme subwavelength electric GHz metamaterials," *J. Appl. Phys.* **110**(5), 054906 (2011).
23. T. J. Cui, "Microwave metamaterials," *Natl. Sci. Rev.* **5**(2), 134–136 (2018).
24. X. Wu, G. V. Eleftheriades, and T. E. van Deventer-Perkins, "Design and characterization of single-and multiple-beam mm-wave circularly polarized substrate lens antennas for wireless communications," *IEEE Trans. Microwave Theory Tech.* **49**(3), 431–441 (2001).
25. R. M. H. Bilal et al., "On the specially designed fractal metasurface-based dual-polarization converter in the THz regime," *Results Phys.* **19**, 103358 (2020).
26. V. S. Asadchy et al., "Broadband reflectionless metasheets: frequency-selective transmission and perfect absorption," *Phys. Rev. X* **5**, 031005 (2015).
27. M. F. Imani, D. R. Smith, and P. del Hougne, "Perfect absorption in a disordered medium with programmable meta-atom inclusions," *Adv. Funct. Mater.* **30**(52), 2005310 (2020).
28. N. I. Landy et al., "Perfect metamaterial absorber," *Phys. Rev. Lett.* **100**(20), 207402 (2008).
29. X. Huang et al., "Polarization-independent and angle-insensitive broadband absorber with a target-patterned graphene layer in the terahertz regime," *Opt. Express* **26**(20), 25558–25566 (2018).
30. F. Chen, Y. Cheng, and H. Luo, "A broadband tunable terahertz metamaterial absorber based on single-layer complementary gammadion-shaped graphene," *Materials* **13**(4), 860 (2020).
31. Y. Cheng, F. Chen, and H. Luo, "Plasmonic chiral metasurface absorber based on bilayer fourfold twisted semicircle nanostructure at optical frequency," *Nanoscale Res. Lett.* **16**(1), 12 (2021).
32. R. M. H. Bilal et al., "Ultrathin broadband metasurface-based absorber comprised of tungsten nanowires," *Results Phys.* **19**, 103471 (2020).
33. R. M. H. Bilal et al., "Triangular metallic ring-shaped broadband polarization-insensitive and wide-angle metamaterial absorber for visible regime," *J. Opt. Soc. Am. A* **39**(1), 136–142 (2022).
34. P.-A. Yang et al., "Excellent microwave absorption performances of high length-diameter ratio iron nanowires with low filling ratio," *Nanotechnology* **31**(39), 395708 (2020).
35. Q. Wang and Y. Cheng, "Compact and low-frequency broadband microwave metamaterial absorber based on meander wire structure loaded resistors," *Int. J. Electron. Commun.* **120**, 153198 (2020).
36. I. S. Maksymov et al., "Optical Yagi-Uda nanoantennas," *Nanophotonics* **1**(1), 65–81 (2012).
37. A. Pattanayak et al., "Study of THz-plasmon hybridization of a loop Yagi-Uda absorber," *Sci. Rep.* **7**, 16961 (2017).
38. R. M. H. Bilal et al., "Polarization-controllable and angle-insensitive multiband Yagi-Uda-shaped metamaterial absorber in the microwave regime," *Opt. Mat. Express* **12**, 798–810 (2022).
39. Y. Arakawa, "The design of liquid crystalline bistolane-based materials with extremely high birefringence," *RSC Adv.* **6**, 92845–92851 (2016).
40. R. Dąbrowski, P. Kula, and J. Herman, "High birefringence liquid crystals," *Crystals* **3**(3), 443–482 (2013).
41. Y. Arakawa et al., "Synthesis of diphenyl-diacetylene-based nematic liquid crystals and their high birefringence properties," *J. Mater. Chem.* **22**(17), 8394–8398 (2012).
42. O. Yaroshchuk and Y. Reznikov, "Photoalignment of liquid crystals: basics and current trends," *J. Mater. Chem.* **22**(2), 286–300 (2012).
43. P. Hirankittiwong et al., "Optical manipulation of the nematic director field around microspheres covered with an azo-dendrimer monolayer," *Opt. Express* **22**, 20087–20093 (2014).

Downloaded From: https://www.spiedigitallibrary.org/journals/Journal-of-Optical-Microsystems on 19 Sep 2023
Terms of Use: https://www.spiedigitallibrary.org/terms-of-use

44. G. Palermo et al., "Optical control of plasmonic heating effects using reversible photo-alignment of nematic liquid crystals," *Appl. Phys. Lett.* **109**(19), 191906 (2016).

Ivan Yakovkin is a PhD student at Taras Shevchenko National University of Kyiv, specializing in liquid crystals. He received his BSc and MSc degrees from the same institution. His research primarily focuses on the reorientation of nematic liquid crystals under external fields and their role in tuning plasmon resonances. Additionally, his research interests include solar astrophysics and machine learning approaches for spectrum processing.

Victor Reshetnyak is a full professor at Taras Shevchenko National University of Kyiv. He received his MSc, PhD, and DSc degrees from Taras Shevchenko National University of Kyiv. He has co-authored more than 270 refereed international book chapters and journal articles and 12 international patents. His research interests include tunable liquid crystal lenses, filled liquid crystals, surface, localized and Tamm plasmons, linear and nonlinear optics of liquid crystals, photorefraction.

Downloaded From: https://www.spiedigitallibrary.org/journals/Journal-of-Optical-Microsystems on 19 Sep 2023
Terms of Use: https://www.spiedigitallibrary.org/terms-of-use